A CURVATURE STRUCTURED TENG FOR HARVESTING ELECTRICAL ENERGY FROM HUMAN MOTION

Cosmina CHIUJDEA [1], Sorin CANANAU [2]

Energy harvesting is the process of collecting energy from the surrounding environment that would otherwise be lost and converting it into electrical power. The generating sources can be mechanical, thermal, radiant or biochemical. The obtained power can then be used to run various small wireless electronic devices. Human motion energy harvesting is a substantial energy source, and triboelectricity, the generation of charges when certain materials come into conformal contact and then separated, is an efficient method for capturing it. In this paper, that methods are explained and a triboelectric nanogenerator (TENG) device driven by human locomotion is implemented and modeled using the Finite Element Method (FEM).

Keywords: energy harvesting, tribocharging, contact electrification, sensors, biomechanical energy harvesting, TENG

1. Introduction

The current energy crisis and ecological harm represent a global issue that is triggered largely by the increased consumption of non-renewable energy sources. This sparked a high interest in the search of alternative energy harvesting technologies, those that prevent exhausting the limited natural resources. Energy harvesting poses as one of the most significant arising sustainable energy solutions today as it can reduce the greenhouse gas emissions, air and water pollution, and environment destruction generated by conventional energy sources.

The types of energy resources available are: fossil fuels, nuclear and renewable resources. The renewable energy sources can be described as those which can be utilized to produce energy consistently, such as photovoltaic energy, wind energy, bioenergy, geothermal energy etc. The difference between renewable energy sources and energy harvesting is that the latter retrieves environmentally derived energy for instant, local use. It is usually used for small systems that only require amounts of power in the range from nanowatts to hundreds of milliwatts, whereas renewable energy sources can facilitate in the charging systems for anything from machinery and tools, electric vehicles or buildings to otherwise entire cities.

[1] PhD. student, Doctoral School of Industrial Engineering and Robotics, National University of Science and Technology POLITEHNICA Bucharest, Romania, e-mail: cosmina.chiujdea@upb.ro
[2] Prof., Faculty of Mecanical Engineering and Mechatronics, National University of Science and Technology POLITEHNICA Bucharest, Romania, e-mail: sorin.cananau@upb.ro

Energy harvesting is the process of collecting energy from the surrounding environment, that would otherwise be lost and converting it into electrical power. The generating sources can be mechanical, thermal, radiant or biochemical. The obtained power can then be used to run various small wireless electronic devices. Each application utilizes a different type of energy harvesting method, depending on factors like the type and amount of available ambient energy, its size limitations and the setting in which the device is operated. Different sources have their own sets of strengths and weaknesses, and one could be a more suitable option than others depending on the context. Lately, the trend of miniaturization of consumer electronics and the spread of the Internet of Things technologies have been a huge proponent of energy harvesting solutions.

The most prevalent ambient energy that can be captured and converted into valuable electric power is mechanical energy. The motion, flow, vibration and pressure generated by a source can be transformed into electrical energy through mechanical to electrical transduction.

2. Mechanical energy harvesting

Energy harvesting efficiency $E_{\%}$ (3) can be determined as the percentage of the power consumed on the external load resistance E_e (2) relative to the total input mechanical power E_m (1):

$$E_m = \int_0^{\Delta t} Fd(t)dt \tag{1}$$

$$E_e = P\Delta t = \frac{V^2}{R}\Delta t \tag{2}$$

$$E_{\%} = \frac{E_e}{E_m}100 \tag{3}$$

where F is the applied force, d is the distance caused by F , Δt is the total time of motion, P is the output power, V is the output voltage, and R is the resistive load applied to the harvester. [1]

Mechanical energy harvesting can be done through piezoelectric, triboelectric, electromagnetic and electrostatic harvesting technologies.

The electromagnetic approach uses the principle of Faraday's law of induction in which the mechanical motion prompts a permanent magnet inside the device to cut through magnetic sensing lines and generate electrical energy.

The electrostatic converters are capacitive devices in which energy conversion takes place as the plates of a variable capacitor separate or the area of the plates is modified in response to externally applied mechanical energy.

The piezoelectric and triboelectric energy harvesting technologies are sparking greater interest for harvesting ambient energy thanks to their many

advantages such as cost effectiveness, simple structure, easy fabrication, lightweight design etc.

Piezoelectric energy harvesting converts motion into electrical energy through piezoelectric materials subjected to mechanical stress, which generate opposite charges on their corresponding surfaces, through the coupling effect between the material's dielectric properties and elasticity.

2.1. Tribocharging

Contact electrification, more commonly known as static electricity (Fig.1), is the process in which charges are generated at the interface between different materials when they are separated, after being brought into contact.

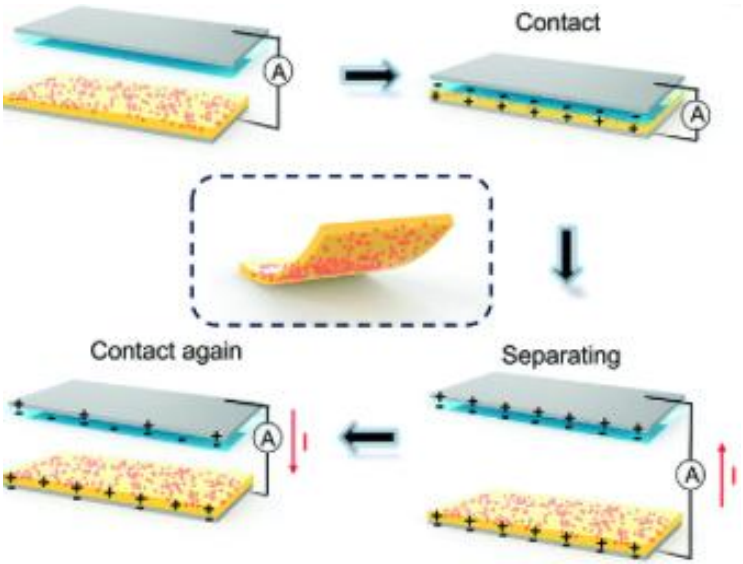

Fig. 1. Working mechanism of the contact–separation mode TENG. When the two triboelectric layers come into contact, opposite charges accumulate on their surfaces. Upon separation, charge redistribution occurs only through the external conductive path (connected to the ammeter), resulting in an induced current. The cycle repeats when the layers come into contact again.

Tribocharging is a particular type of contact electrification that occurs through frictional interaction. Unlike simple contact electrification, which results from contact and separation alone, tribocharging uses mechanical friction to increase charge accumulation through repeated contact instances. The amount of generated charge is conditioned by many factors, such as humidity, external temperature, impact velocity, flow density, material composition etc. The fundamental mechanism of tribocharging is still a subject of active research, with several competing models attempting to explain charge transfer. These include the electron transfer model, which suggests that charge is exchanged through

differences in work function [2], the ion transfer model, which attributes charging to mobile ions at material surfaces [3], and the material transfer theory, which proposes that microscopic material fragments contribute to charge buildup [4].

Table 1

Different triboelectric series

	Series 1	Series 2	Series 3	Series 4	Series 5	Series 6	Series 7
Donor of electrons Acquires positive charge	Human hands						
	Asbestos			Lucite 2041			
	Rabbit's Fur			Dapon			Nylon 6.6
	Acetate			Lexan 105	Plexiglass		Cellulose
	Glass			Formvar	Bakelite	Rabbit's Fur	Cellulose Acetate
	Mica			Estane	Cellulose Acetate	Lucite	Polymethyl Methacrylate
	Human hair		Polyox	DuPont 49000	Glass	Bakelite	Polyacetal
	Nylon	Wool	Polyethylene Amine	Durex	Quartz	Cellulose	Polyethylene Terephthalate
	Wool	Nylon	Gelatin	Ethocel 10	Nylon	Acetate	Polyacrylonitrile
	Fur	Viscose	Vinac	Polystyrene 8X	Wool	Glass	Polyvinyl Chloride
	Lead	Cotton	Lucite 44	Epolene C	Silk	Quartz	Polybisphenol Carbonate
	Silk	Silk	Lucite 42	Polysulphone P-3500	Cotton	Mica	Polychloroether Penton
	Aluminum	Acetate	Acryloid A101	Hypalon 30	Paper	Wool	Polyvinylidine Chloride
	Paper	Rayon	Zelec DX	Cyclolac H-1000	Amber	Cat's Fur	Poly2.6-Dimethyl Polyphenylene Oxide
	Cotton	Lucite, Perspex	Polyacrylamide	Uncoated Iron	Resins	Silk	Polystyrene
	Steel	Polyvinyl Alcohol	Cellulose Acetate/ Butyrate	Cellulose Acetate Butyrate	Metals	Cotton	Polyethylene
	Wood	Dacron	Acysol	Epon 828/V125	Rubber	Wood	Polypropylene
	Amber	Orlon	Carbopol	Polysulphone P-1700	Acetate Rayon	Amber	Polytetrafluoroethylene
	Hard rubber	PVC	Polyethylene terephthalate	Cellulose Nitrate	Dacron	Resins	
	Mylar	Dynel	Polyvinyl Butyral	Kynar	Orlon	Metals	
	Nickel, Copper	Velon	Polyethylene		Polystyrene	Polystyrene	
	Silver	Polyethylene			Teflon	Polyethylene	
	UV Resist	Teflon			Cellulose Nitrate	Teflon	
	Brass, Stainless Steel				PVC	Cellulose Nitrate	
	Gold						
	Polyester						
	Celluloid						
	Styrene						
Acceptor of electrons Acquires negative charge	Acrylic						

A critical challenge in studying triboelectric charging lies in accurately measuring and correlating tribological parameters with charge generation. Existing studies often rely on simplified experimental conditions that do not fully capture the complexity of real-world interactions.

Through experimental methods it was discovered that the polarity of the electric charge directly depends on the properties of the material. Based on this, a classification of materials was developed, known as the triboelectric series, in order to predict the polarity of materials charged by contact.

Shaw [5] developed the first triboelectric series in 1917. In his experiments he used an electroscope to measure the charge generated at the surface of various tested materials rubbed together. This classification allows the materials to be ordered from the one that is most positively charged to the one that is most negatively charged. In a triboelectric series, the more two materials are apart in the ranking, the more significant the charge transfer generated between them is.

Over the years, several triboelectric series have been developed as shown in Table 1. These series were obtained by different methods and different experimental conditions, which justifies the lack of a universal triboelectric series.

Wilke [6] presented a triboelectric series (Table 1. Series 1) that indicates the polarity of the charge generated after a sliding or rolling contact between two arbitrary materials. The ranking of materials in the series can differ depending on several factors, such as surface roughness, material purity, humidity, effective contact area during friction.

2.2. Biomechanical energy

A typical human body is capable to utilize between 7 and 10 MJ of energy per day, and up to 17 MJ in the cases of triathletes [7]. The majority of this energy is used for essential tasks, such as heart pumping or muscle flexing. Nevertheless a lot of it is lost, mainly as heat. The power lost in a human body is considerably higher than the power consumption of wearable and mobile devices, accounting that 10MJ of energy could power an electric car for 10–15 km.

Many studies have demonstrated the potential of biomechanical energy harvesting technologies. Cheng et. al. [8] developed a stretchable integrated nanogenerator with a coaxial core-sheath fiber architecture.. The solution allows energy harvesting from a vast range of motions from stretching, joint bending, twisting and pressing, to subtle signals such as breath, pulse or even speech.

Kuang et al. [9] designed a portable two-dimensional rotary triboelectric nanogenerator as a portable and wearable power source for electronics. Enabled by a design of two radial-arrayed fine electrodes that are complementary on the same plane, the planar-structured r-TENG harvesting energy from either foot pedaling, arm swinging or foot pressure. A very similar solution was introduced by Segkos et al. [10].

3. The curvature structured triboelectric nanogenerator

The C-TENG device (Fig.2) presented by Wang and Feng [11] utilizes the curvature effect to enhance the mechanical energy harvesting efficiency. It features

a supporting structure composed of a flexible base, a rigid base, and two elastic support elements. Both the flexible and rigid substrates have curved surfaces designed to hold conductive electrodes and triboelectric materials. The triboelectric pair consists of a 50 µm thick PTFE film and a 70 µm thick nylon film, each measuring 2 × 4 cm². Aluminum foil is used as a conductive electrode, attached to the back of the triboelectric layers.

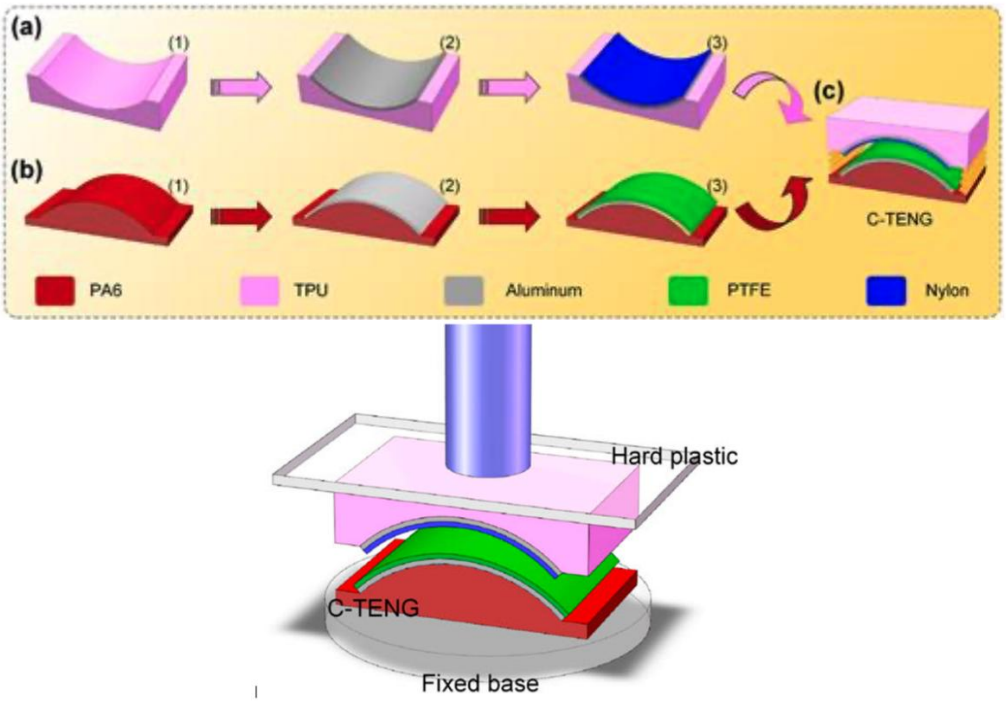

Fig. 2. C-TENG device : (a1)–(a3) the concave curved flexible substrate; (b1)–(b3) the convex curved flexible substrate.

The device was designed to be integrated into the sole of a shoe, with the purpose of harvesting biomechanical energy generated during locomotion. In its current configuration, the elastic support elements play a critical role, as the TENG's performance—specifically the amount of electrical energy harvested—is closely linked to the layers' ability to repeatedly come into contact and separate, in accordance with the principles of contact electrification. It is essential that these supports withstand the high-impact forces associated with walking, running, jumping, or dancing, while also exhibiting sufficient elasticity to return to their original shape after repeated deformation cycles.

The 3D model, illustrated in Figure 3, was designed to simulate the behavior of the device using elastic supports made from various materials. Figure 4 presents

the computational domain and the Finite Element Method (FEM) mesh of the portable device.

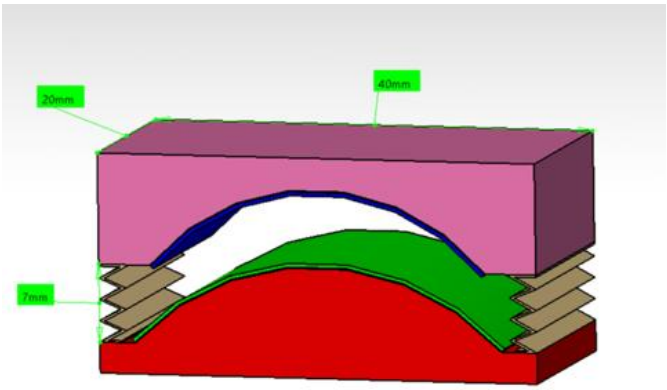

Fig. 3. CAD Model of C-TENG

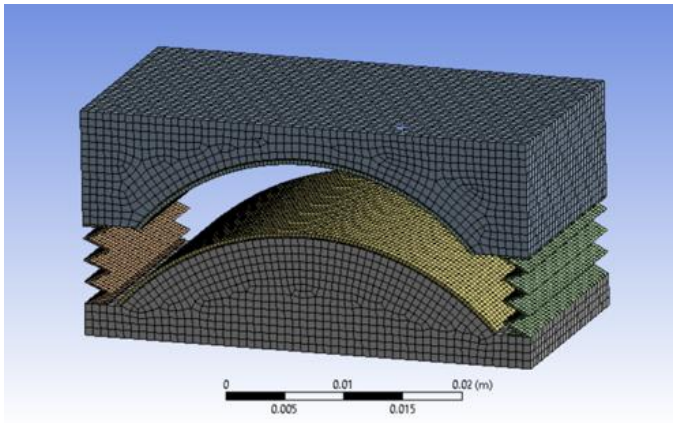

Fig.4. The computational domain and the FEM mesh.

The mathematical model was solved using the FEM technique, as implemented by [12].

3.1. The electrical output of the device

The data summarized in Tables 2–5 are taken from the study of Wang and Feng [11] which reports the mechanical and electrical characteristics of the curvature-structured TENG. The original publication provides the numerical and experimental methodology used to obtain these results.

The device's performance can be seen in tables 2 ,3, 4 and 5, where V_{oc} is the open-circuit voltage, I_{sc} is the short-circuit current and Q_{sc} is the transfer charge.

Table 2

C-TENG Performance improvement effect brought by the curvature

Structure Type	V_{oc} (V)	I_{sc} (µA)	Q_{sc} (nC)
P-TENG (Flat)	234.61	12.25	71.96
C-TENG (Curved)	347.46	20.31	98.91
Flipped C-TENG	186.64	9.17	56.76

Table 3

C-TENG Output depending on the flexible component hardness

Hardness (°Shore A)	V_{oc} (V)	I_{sc} (µA)	Q_{sc} (nC)
90	217.07	16.07	45.86
60	399.35	35.47	101.18
30	315.89	26.95	86.63

Table 4

C-TENG Output depending on the curvature of the rigid component

Curvature (K)	V_{oc} (V)	I_{sc} (µA)	Q_{sc} (nC)
0.01	333.04	25.31	55.15
35	548.35	55.81	109.11

Table 5

C-TENG Output depending on the relative humidity

Humidity (%)	V_{oc} (V)	I_{sc} (µA)	Q_{sc} (nC)
30	403.45	18.14	110.66
60	191.75	37.63	68.54

The C-TENG was tested using three sensors placed on a flexible surface: Sensor 1 at the toe, Sensor 2 at the midfoot, and Sensor 3 at the heel. Figure 5 shows how each sensor responds to different mechanical excitations. When a rigid plate uniformly pressed the surface (top-left), all sensors produced nearly identical outputs, confirming uniform contact. When force was applied at a specific position—toe (top-right), midfoot (bottom-left), or heel (bottom-right)—the corresponding sensor generated the highest voltage, current, and charge.

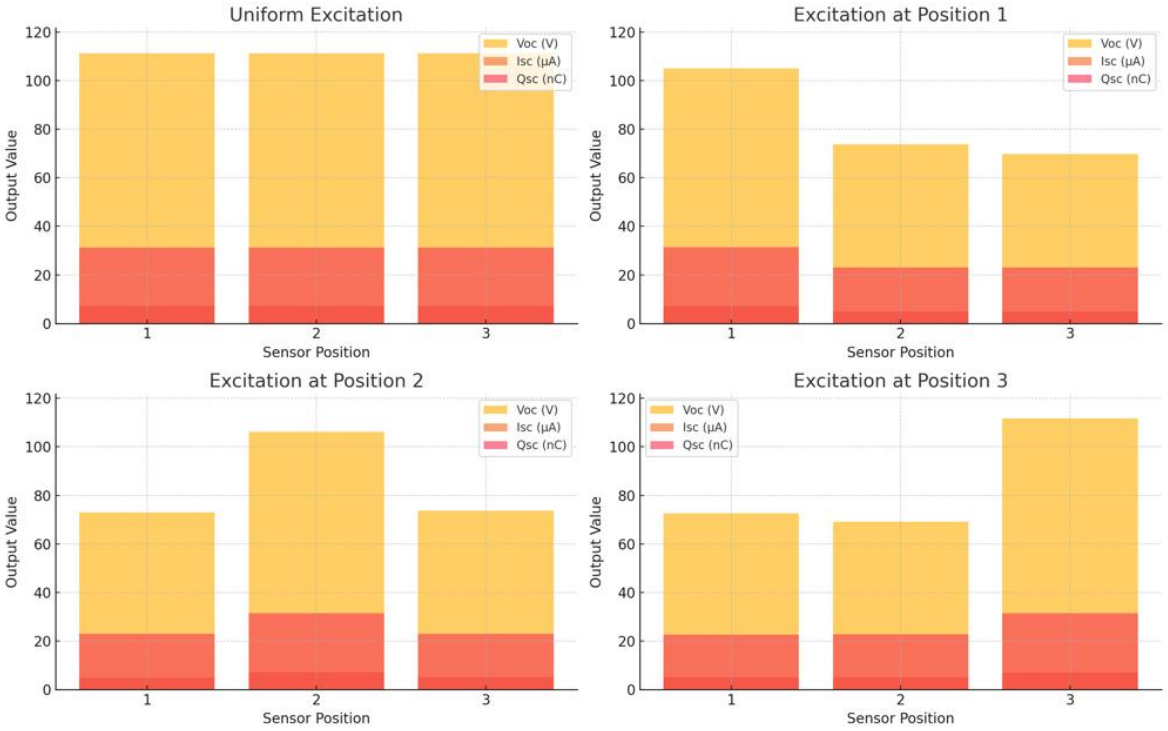

Fig. 5. The output of the C-TENG sensors under different excitation conditions.

4. Results and discussion

The deformation of the TPU elastic support under external pressure was modeled assuming linear elastic behavior. The strain–displacement relation is:

$$\varepsilon = \frac{1}{2}(\Delta u + \Delta u^T) \tag{4}$$

The constitutive equation for isotropic elasticity is:

$$\sigma = C\varepsilon \tag{5}$$

where C is the elasticity matrix defined by Young's modulus E and Poisson's ratio ν.

The equivalent von Mises stress, used to evaluate yielding behavior, is computed as:

$$\sigma_\nu = \sqrt{\frac{1}{2}[(\sigma_x - \sigma_y)^2 + (\sigma_y - \sigma_z)^2 + (\sigma_z - \sigma_x)^2] + 3(\tau_{xy}^2 + +\tau_{yz}^2 + \tau_{zx}^2)} \tag{6}$$

To evaluate the behavior of the TPU-based elastic support component in the C-TENG structure, static structural simulations were performed in ANSYS for three different applied pressures: 0.8 MPa, 1.0 MPa, and 1.5 MPa. The pressures simulate contact forces representative of varying human body weights during normal

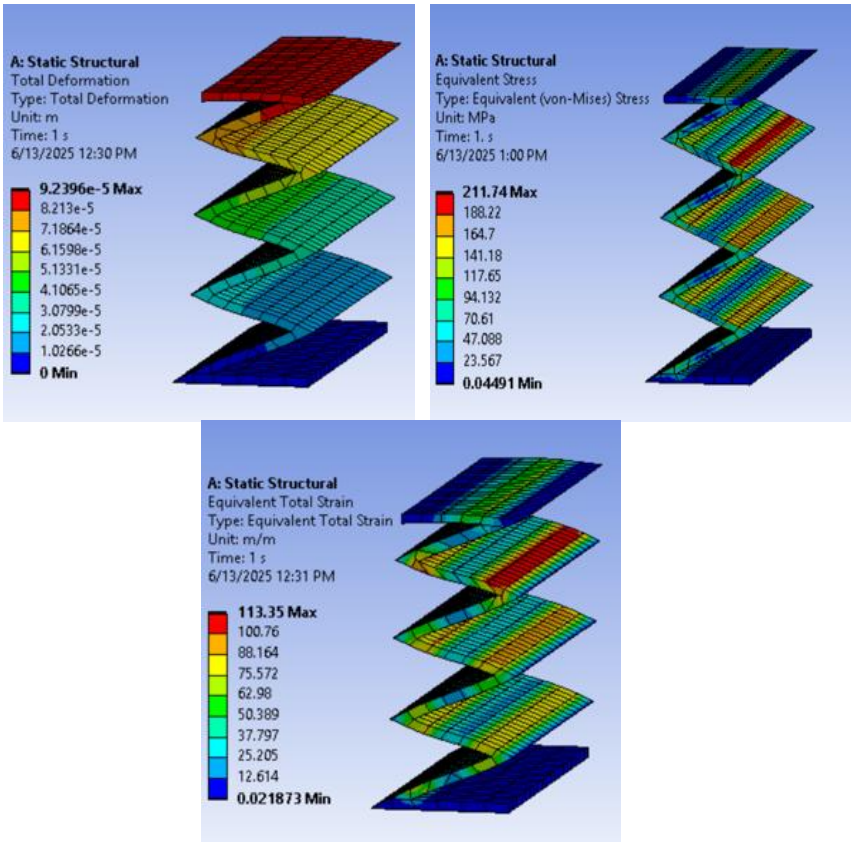

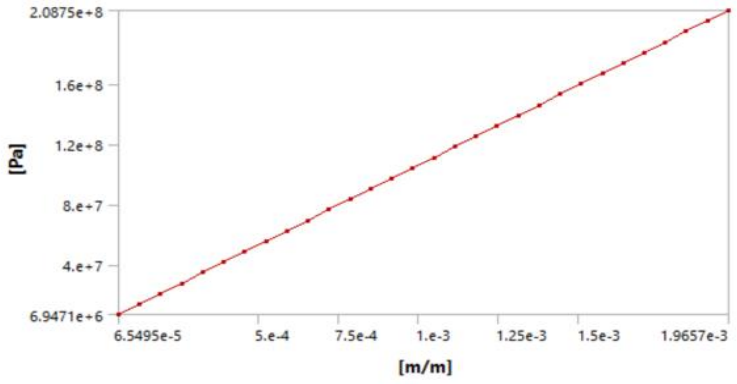

Fig. 6. Simulation results for the TPU elastic support under 0.8 MPa pressure: total deformation, equivalent (von Mises) stress, equivalent (von Mises) strain and stress–strain response.

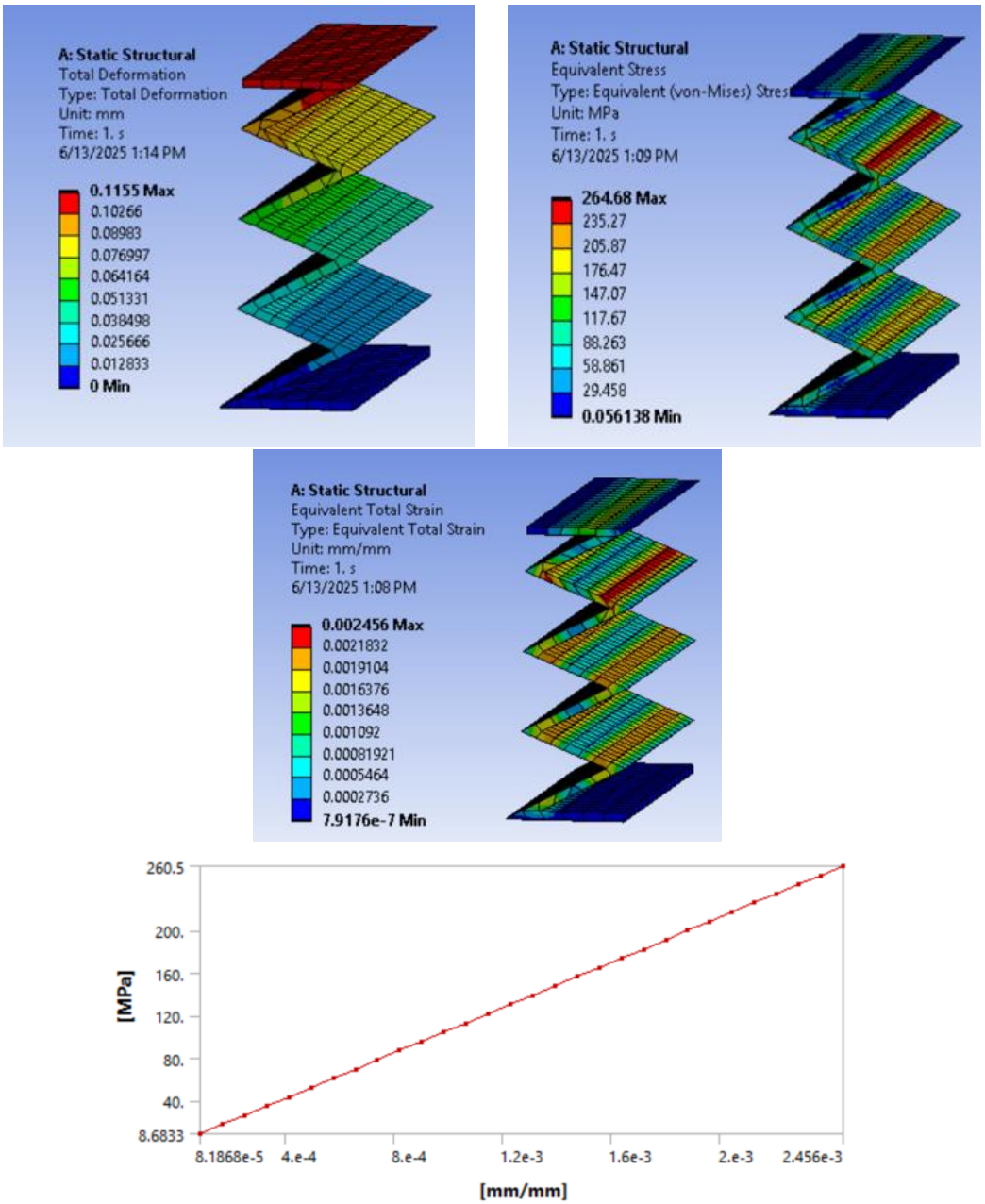

Fig. 7. Simulation results for the TPU elastic support under 1 MPa pressure: total deformation, equivalent (von Mises) stress, equivalent (von Mises) strain and stress–strain response.

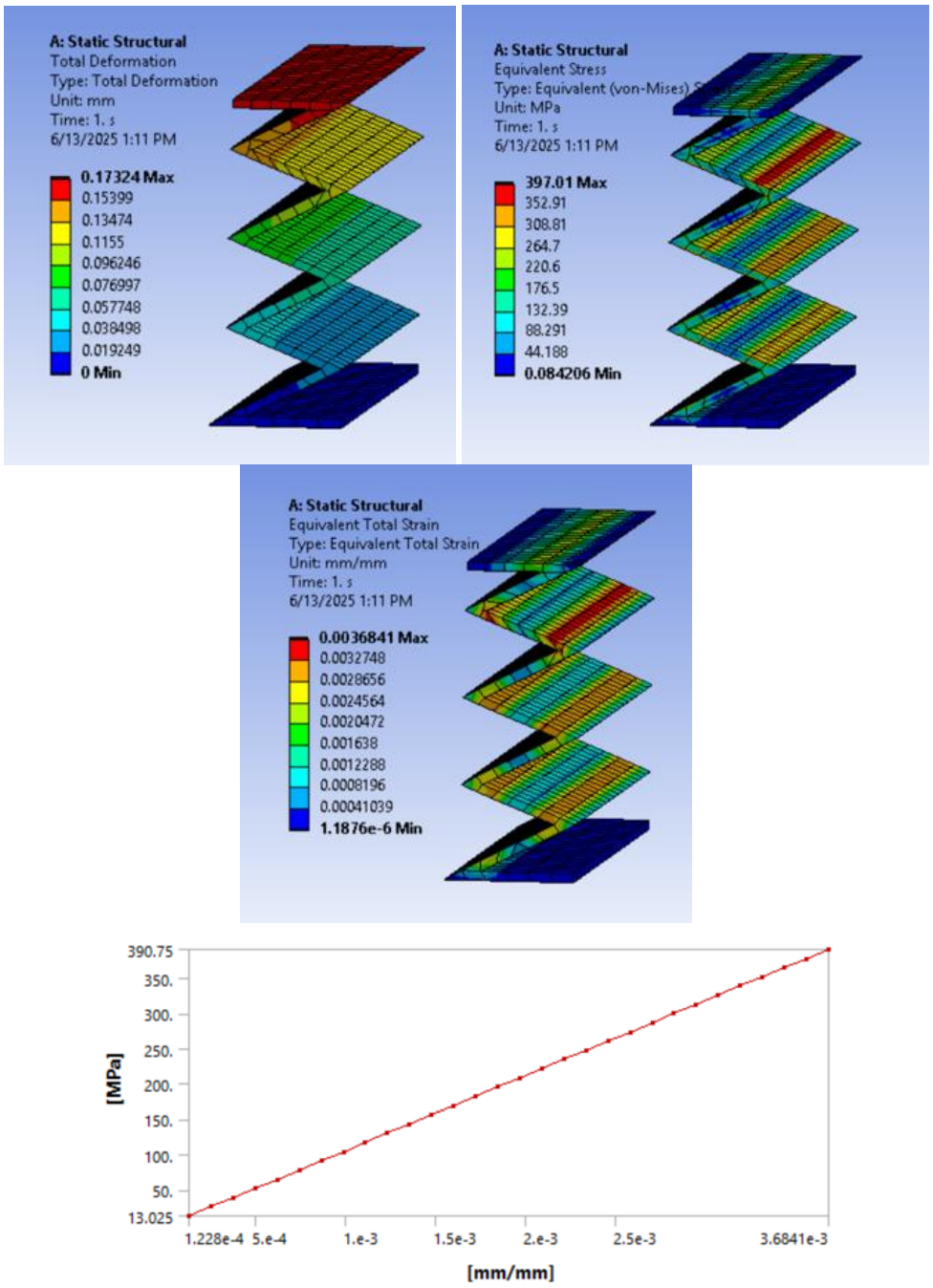

Fig. 8. Simulation results for the TPU elastic support under 1.5 MPa pressure: total deformation, equivalent (von Mises) stress, equivalent (von Mises) strain and stress–strain response.

The total deformation increased with applied pressure, showing a non-linear yet predictable elastic response. Under 0.8 MPa, the elastic support exhibited

moderate deflection, remaining within the expected range of recoverable deformation for TPU. At 1.5 MPa, deformation increased significantly, but the structure did not show signs of instability or failure, indicating good mechanical compliance and resilience of the support.

This response is consistent with TPU's high elongation capacity and elasticity. However, deformation at higher loads approached the upper limit of the acceptable working range, which may affect long-term performance if frequent high loads are expected.

Stress and strain levels followed an expected trend with load increase, showing some local regions within the support exhibited stress values near the yield threshold.

Strain distributions showed TPU's ability to accommodate large deformations without material failure. Even at the highest pressure, the strain remained below the critical strain value typically associated with failure or cracking for TPU.

The extracted stress–strain curve reflects typical elastomeric behavior with a smooth transition from elastic to plastic deformation. The response was predominantly linear.

The TPU support demonstrated good strain-hardening behavior, maintaining structural integrity even beyond the yield point. However, repeated cycling at this level could lead to fatigue accumulation, particularly in regions of stress concentration.

5. Conclusions

The portable device presented in this paper is both versatile and flexible. It can be used in a variety of activities and by individuals of different body sizes and activity levels, ranging from very active to more sedentary, while still generating enough electrical energy to power electronic devices. The device is also scalable and can be adapted to accommodate various shoe sizes.

From the simulation, TPU proves to be a suitable material for the elastic support in the C-TENG, especially under moderate loads. It provides enough flexibility to maintain full contact between triboelectric layers while withstanding reasonable stress levels without failure.

To ensure durability under diverse body weights, particularly in wearable or weight-sensitive applications, it is advisable to consider increasing the cross-sectional area of the support to reduce local stress, use a stiffer TPU variant or composite for high-load zones, or limit the maximum load through mechanical stops or design constraints.

Further work using fatigue analysis or dynamic simulations could offer better insight into the long-term performance under repeated load cycles.

REFERENCES

[1] J. Y. Cho *et al.*, "A multifunctional road-compatible piezoelectric energy harvester for autonomous driver-assist LED indicators with a self-monitoring system," *Applied Energy*, vol. 242, pp. 294–301, May 2019.

[2] D. Tan, M. Willatzen, and Z. L. Wang, "Electron transfer in the contact-electrification between corrugated 2D materials: A first-principles study," *Nano Energy*, vol. 79, p. 105386, Jan. 2021, doi: 10.1016/j.nanoen.2020.105386.

[3] A. F. Diaz and D. Fenzel-Alexander, "An ion transfer model for contact charging," *Langmuir*, vol. 9, no. 4, pp. 1009–1015, Apr. 1993.

[4] R. Pandey, H. Kakehashi, H. Nakanishi, and S. Soh, "Correlating Material Transfer and Charge Transfer in Contact Electrification," *The Journal of Physical Chemistry C*, vol. 122, Jul. 2018.

[5] P. E. Shaw., "Experiments on Tribo-Electricity. I. The Tribo-Electric Series.," *Proceedings of the Royal Society of London*, vol. 94, no. 656, pp. 16–33, 1917.

[6] J. C. Wilcke, *Disputatio physica experimentalis, de electricitatibus contrariis*. Rostochii: Typis Ioannis Iacobi Adleri, 1757.

[7] C. Williams, "Dietary macro- and micronutrient requirements of endurance athletes," *The Proceedings of the Nutrition Society*, vol. 57, pp. 1–8, Feb. 1998.

[8] Y. Cheng *et al.*, "A stretchable fiber nanogenerator for versatile mechanical energy harvesting and self-powered full-range personal healthcare monitoring," *Nano Energy*, vol. 41, pp. 511–518, Nov. 2017.

[9] S. Y. Kuang, J. Chen, X. B. Cheng, G. Zhu, and Z. L. Wang, "Two-dimensional rotary triboelectric nanogenerator as a portable and wearable power source for electronics," *Nano Energy*, vol. 17, pp. 10–16, Oct. 2015.

[10] A. Segkos and C. Tsamis, "Rotating Triboelectric Nanogenerators for Energy Harvesting and Their Applications," *Nanoenergy Advances*, vol. 3, no. 3, Art. no. 3, Sep. 2023.

[11] J. Wang and A. Feng, "Curvature structure triboelectric nanogenerator for harvesting human motion energy and cheerleading training monitoring," *AIP Advances*, vol. 14, no. 12, p. 125130, Dec. 2024.

[12] ***, ANSYS – Finite Element Analysis, Release 19.0 User Guide, 2018.

[13] L. Lang, R. Antunes, T.A. Dutra, M.L. Aguiar, N. Pereira, P.D. Gaspar, "Mechanical Characterization and Computational Analysis of TPU 60A: Integrating Experimental Testing and Simulation for Performance Optimization" *Materials*, vol. 18, no. 2, p. 240, 2025.